in the sense that the corresponding wave suffers absorption when it propagates into a semi-infinite crystal (Miyake, 1969). 1′ and 2 branches are not realistic because the corresponding wave suffers intensity enhancement in the crystal. The dashed curve 3 gives $Z' \geq 0$ and is unrealistic, so that the realistic branch starting from curve 1 for $W > 1$ leaves the hyperbola at $W = 1$ and follows the curve 3′. It leaves curve 3′ at $W = -1$ and follows the curve 2′. In a similar manner, in Fig. 5(*e*), for the realistic branch, the real part is given by curve 1 for $W > -1$ and by curve 2′ for $W < -1$. The imaginary part of the realistic branch always stays in the lower half of the dashed curve. If we compare the realistic branches in (*a*) and (*e*), they have a similar form. In Fig. 6(*e*), the diffracted intensity does not have a top-hat form and has the maximum near $W = -1$ when $Z' = 0$. The total reflection occurs at one point near $W = -1$.

5. Summary

We have studied dispersion surfaces by changing the ratio between the real and imaginary parts of the X-ray polarizability. It is shown that the dispersion surface in the symmetric Laue case for no real part of the polarizability ($q = 1$) is quite different from the well known form of the dispersion surface when the imaginary-part polarizability is zero. It shows a similar form to that in the symmetric Bragg case for no imaginary part of the polarizability. The dispersion surface in the Laue case for $q = 1$ becomes pure imaginary for $-1 < W < 1$, which explains why the abnormal transmission and absorption effects result.

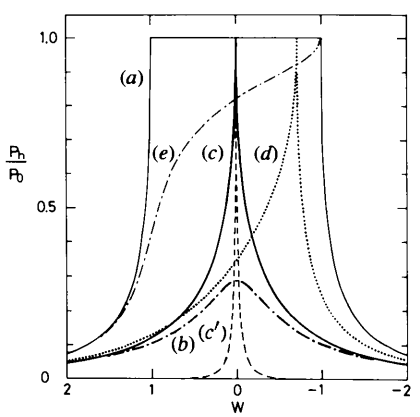

Fig. 6. The rocking curves in the symmetric Bragg case. The conditions for curves (*a*)–(*e*) correspond to those in Fig. 5. The details for curve (*c*′) are given in the text.

In the symmetric Bragg case from a semi-infinite crystal, the dispersion surface for no real part of the polarizability has no gap between the two branches and the two branches are tangential to each other at $W = 0$. This results in a very sharp rocking curve when the real-part polarizability is zero. The sharp rocking curve may be useful for a monochromator with small divergent angle. As an example, Fig. 6(*c*′) shows the rocking curve after four times diffraction from such a channel-cut monochromator. The width of the rocking curve (*c*′) is 1/100 of the curve (*a*).

As shown above, the complex dispersion surfaces for various values of q are quite useful to interpret not only the shapes of the rocking curves but also the abnormal transmission and absorption effects. It is also possible to obtain information on the phases of waves corresponding to each branch point by using the dispersion surface. A paper on this topic will be published in the near future.

References

FUKAMACHI, T. & KAWAMURA, T. (1993). *Acta Cryst.* A**49**, 384–388.
FUKAMACHI, T., NEGISHI, R., YOSHIZAWA, M., EHARA, K., KAWAMURA, T., NAKAJIMA, T. & ZHAO, Z. (1993). *Acta Cryst.* A**49**, 573–575.
JAMES, R. W. (1963). *Solid State Phys.* **15**, 53–220.
KATO, N. (1992). *Acta Cryst.* A**48**, 829–833.
MIYAKE, S. (1969). *X-ray Diffraction*. Tokyo: Asakura. (In Japanese.)
PINSKER, Z. G. (1978). *Dynamical Scattering of X-rays in Crystals*. New York: Springer.
ZACHARIASEN, W. H. (1945). *Theory of X-ray Diffraction in Crystals*. New York: Dover.

Acta Cryst. (1995). A**51**, 258–268

Darwin Spherical-Wave Theory of Kinematic Surface Diffraction

BY S. M. DURBIN

Department of Physics, Purdue University, West Lafayette, IN 47907, *USA*

(*Received* 5 *April* 1994; *accepted* 7 *September* 1994)

Abstract

In 1912, von Laue first described X-ray diffraction by approximating as plane waves the spherical waves radiated by atoms in a crystal. Darwin recognized that this approximation is valid only in the limit of very small crystals, and published in 1914 the more general spherical-wave theory based on the reflectivity of individual atomic planes. The Darwin theory is extended here to surface Bragg diffraction from a single-crystalline

©1995 International Union of Crystallography
Printed in Great Britain – all rights reserved

monolayer, including the rederivation of a 'surface' Bragg's law and the reflected intensity *versus* φ, the angle of incidence. This more general theory demonstrates how the intensity along a reciprocal-lattice rod associated with diffraction from a semi-infinite crystal is modified by the φ dependence of the length over which atoms in a plane emit spherical waves that constructively interfere at the detector. The diffracted amplitude is not proportional to the Fourier transform of the charge density. The plane- and spherical-wave models yield identical results for the integrated intensity across a finite detector area, even for incident angles far from a Bragg reflection.

I. Introduction

The sensitivity of X-ray diffraction measurements has increased enormously since the original discovery of von Laue over eight decades ago (Friedrich, Knipping & von Laue, 1913; von Laue, 1913). For much of this time, diffraction data have been largely used by crystallographers to determine within a few percent the integrated intensity of a reflection, from which atomic structure can be inferred. With today's more sophisticated equipment and especially synchrotron-radiation sources, the previously undetectable 'tails' of a Bragg reflection are measured at levels more than a million times weaker than the Bragg-peak intensity and are analyzed to determine the structure of single atomic monolayers at the surface of a crystal (Andrews & Cowley, 1985; Robinson, 1986). As the experimental capabilities have so dramatically improved, it seems worthwhile to re-examine the kinematic theory of X-ray diffraction, which is commonly used in surface crystallography. In the following sections, we have largely restated or rederived the basic results of kinematic theory. While nearly all of the results were originally published long ago, only recently has it become particularly useful to examine the predicted reflectivities far from the Bragg peaks. Using Darwin's original model of spherical-wave diffraction (Darwin, 1914), we show how the scattered amplitudes differ for all angles of incidence between the plane- and spherical-wave theories for monolayer and bulk crystal diffraction. We further show, however, that the equivalence of the Bragg-peak integrated intensities for plane and spherical waves remains valid even in the tails of a Bragg reflection.

X-ray crystallography relies upon deducing the structure factors, $F_{\mathbf{H}}$, which are themselves functions of the positions of the atoms within the crystal unit cell. The scattering density in the crystal, $\rho(\mathbf{r})$, can also be expressed in terms of the structure factors:

$$\rho(\mathbf{r}) = (1/V)\sum_{\mathbf{H}} F_{\mathbf{H}} \exp(-2\pi i\, \mathbf{H}\cdot\mathbf{r}), \qquad (1)$$

where the $\mathbf{H}$ are the reciprocal-lattice vectors of the crystal and V is the unit-cell volume. From this, we see that the structure factors are simply Fourier components of the scattering density,

$$F_{\mathbf{H}} = \int \rho(\mathbf{r}) \exp(2\pi i\, \mathbf{H}\cdot\mathbf{r})\mathrm{d}\mathbf{r} = \rho_{\mathbf{H}} \qquad (2)$$

Insofar as an X-ray diffraction measurement determines $F_{\mathbf{H}}$, we say that the Fourier transform of the scattering density has been measured. By measuring $|F_{\mathbf{H}}|$ for a sufficient number of $\mathbf{H}$s and using various strategies for measuring and/or guessing the phases of the structure factors, the complete scattering density $\rho(\mathbf{r})$ can be approximated and the atomic structure of the crystal determined.

As noted by Ewald (1940), for a perfect unbounded crystal, the generalized Fourier transform $F(\mathbf{q})$ is zero except when $\mathbf{q} = \mathbf{H}$, so $F(\mathbf{q})$ is essentially a set of δ functions with area $F_{\mathbf{H}}$ at each node $\mathbf{H}$ of the reciprocal lattice. In other words, $\rho(\mathbf{r})$ can be represented by assigning $F_{\mathbf{H}}$ to each node $\mathbf{H}$. The connection between X-ray diffraction and the Fourier transform of the scattering density is even more apparent when the crystal is finite and so small that the plane-wave approximation can be used (to be discussed below). The scattering density can be written as

$$\rho_s(\mathbf{r}) = \rho(\mathbf{r})s(\mathbf{r}), \qquad (3)$$

where $\rho(\mathbf{r})$ is the scattering-density function for the infinite crystal and $s(\mathbf{r})$ is the crystal-shape function, which is unity when $\mathbf{r}$ is within the crystal boundaries and zero otherwise (Ewald, 1940). The Fourier transform of $\rho_s(\mathbf{r})$ is the convolution of the infinite-crystal δ function with the Fourier transform of the shape function. (For a crystal in the shape of a thin plate, for example, the shape transform will be a thin rod perpendicular to the surface.) If we examine the scattered X-ray intensity as a function of the scattering wave vector $\mathbf{q}$, the plane-wave approximation leads to an $I(\mathbf{q})$ that is proportional to the square of the Fourier transform of $\rho_s(\mathbf{r})$.

The connection between diffraction and the Fourier transform of the scattering density forms a natural and intuitive foundation for much X-ray analysis. We shall see here, however, how this idea breaks down when the plane-wave model is no longer an adequate representation of the spherical waves that are actually emitted by the atoms. In particular, the Fourier transform of a single monolayer is a rod of constant amplitude in reciprocal space, yet the specularly reflected intensity $I(\mathbf{q})$ will be shown below to have a $1/q^2$ dependence in the surface normal direction. This follows simply from the angular dependence of the maximum separation across which atoms can emit spherical waves that constructively interfere at the detector, *i.e.* the diameter of the first Fresnel zone (Darwin, 1914).

This additional factor of $1/q^2$ also appears in diffraction from a semi-infinite crystal. Here, the Fourier transform of the shape function happens to be $1/q$ in the surface normal direction, which corresponds to $1/(\Delta q)^2$

intensity tails about each Bragg peak. In the spherical-wave theory, however, the specularly reflected intensity should fall as $1/q^4$ and as $1/(q^2\Delta q^2)$ from all other reflections. We address these differences because they clearly show that the physics of diffraction for plane and spherical waves is not the same. However, when these differing amplitudes are combined with their corresponding angular dependences to calculate the integrated intensity across the area of an X-ray detector, the errors in the plane-wave model cancel out to yield the correct spherical-wave result. This effect is well known for the peak intensity at a Bragg reflection (James, 1948). We demonstrate here its validity far into the tails of a reflection, where surface crystallography is done.

II. Kinematic theory of diffraction

We compare here the plane-wave and spherical-wave models of kinematic diffraction, with the goal of having a proper physical description of surface diffraction. Absorption is neglected and there is no interaction between the the scattered waves and the crystal, *i.e.* the dielectric constant is unity. The plane-wave model is the original picture used by von Laue (1913) to explain X-ray diffraction from crystals. We present in (*A*) a review of this plane-wave model. The first spherical-wave theory of X-ray diffraction was published by Darwin in 1914, shortly after von Laue's seminal work. [Note also that von Laue included an initial discussion of the spherical-wave theory in von Laue & Tank (1913).] In (*B*), we re-derive Darwin's calculation of the specular reflectivity of a monolayer, which is based on summing the spherical-wave amplitudes radiated by oscillating point charges driven by the incident wave field. Some of the details of this calculation are found in Appendix *A*. We then extend this approach to diffraction from the periodic arrangement of atoms in a crystal monolayer, *i.e.* surface diffraction, with many of the details reserved for Appendix *B*.

(*A*) *Plane waves*

The plane-wave approximation developed by von Laue (1913) can be found in the books by James (1948) and Warren (1969), among others. Consider an isolated atom in vacuum at position $\mathbf{d}_o$ which is illuminated by an electromagnetic plane wave with electric field amplitude $\mathbf{E}_I = \hat{\boldsymbol{\varepsilon}}_I E_I \exp[i(2\pi\mathbf{k}_I \cdot \mathbf{d}_o - \omega t)]$. Here, $k_I = \omega/2\pi c = 1/\lambda$ is the wave vector, and $\hat{\boldsymbol{\varepsilon}}_I$ the unit polarization vector. By treating the atom as an electric dipole, Maxwell's equations determine that radiation will be emitted by the accelerated charges as spherical waves. The amplitude at a point P a displacement $\mathbf{r}$ away is given by the Thomson formula:

$$E_o = -(r_e/r)f\{(E_I \exp[i(2\pi\mathbf{k}_I \cdot \mathbf{d}_o - \omega t)]\} \exp(+i\omega r/c)$$
$$= -(r_e/r)f\tilde{E}_I \exp(2\pi i k r). \quad (4)$$

Here, r_e is the classical electron radius e^2/mc^2, f is the complex atomic scattering factor and $\tilde{E}_I \equiv E_I \exp[i(2\pi\mathbf{k}_I \cdot \mathbf{d}_o - \omega t)]$. For simplicity, we consider only perpendicular polarization, *i.e.* $\hat{\boldsymbol{\varepsilon}}_I \perp \mathbf{r}$. The field at P from an atom displaced from $\mathbf{d}_o$ by the vector $\mathbf{d}_m$ (Fig. 1) is

$$E_m = -(r_e/r')f\tilde{E}_I \exp(2\pi i\,\mathbf{k}_I \cdot \mathbf{d}_m) \exp(i\omega r'/c), \quad (5)$$

where $r' = |\mathbf{r}'| = |\mathbf{r} - \mathbf{d}_m|$. As long as the distance between atoms is small compared to the distance to the detector, the factor r_e/r' can be replaced by r_e/r. In the plane-wave approximation, one further assumes that $\mathbf{r}'$ can be replaced by its projection along $\mathbf{r}$: $r' \simeq r - \mathbf{d}_m \cdot \hat{\mathbf{r}}$. This leads to

$$E_m = -(r_e/r)f\tilde{E}_I \exp(2\pi i\,\mathbf{k}_I \cdot \mathbf{d}_m) \exp[2\pi i\,\mathbf{k} \cdot (\mathbf{r} - \mathbf{d}_m)]$$
$$= -(r_e/r)f\tilde{E}_I \exp(2\pi i\,\mathbf{k} \cdot \mathbf{r}) \exp[2\pi i(\mathbf{k}_I - \mathbf{k}) \cdot \mathbf{d}_m]. \quad (6)$$

The phase of this wave at P is calculated as if the atom at $\mathbf{d}_m$ emits a plane wave traveling parallel to $\mathbf{r}$, the displacement between the atom at $\mathbf{d}_o$ and the detector at P. The amplitude still has the $1/r$ dependence of a spherical wave.

In a crystal, each of the displacements $\mathbf{d}_m$ is a Bravais lattice vector $\mathbf{d}_m = m_1\mathbf{a}_1 + m_2\mathbf{a}_2 + m_3\mathbf{a}_3$ and the atomic scattering factor f is replaced by the structure factor F. The total amplitude at P is the sum of E_ms over all unit cells:

$$E_T = \sum_m E_m$$
$$= -(r_e/r)\tilde{E}_I \exp(2\pi i\,\mathbf{k} \cdot \mathbf{r})F(\mathbf{q})$$
$$\times \sum_{m_1}\sum_{m_2}\sum_{m_3} \exp[2\pi i\mathbf{q} \cdot (m_1\mathbf{a}_1 + m_2\mathbf{a}_2 + m_3\mathbf{a}_3)], \quad (7)$$

where $\mathbf{q} \equiv \mathbf{k}_I - \mathbf{k}$. For a crystal with $N_1N_2N_3$ ($\equiv N$) unit

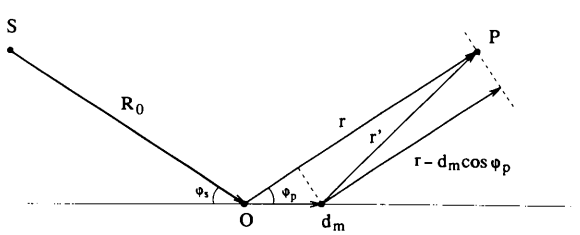

Fig. 1 Scattering geometry for an atom at the origin O and a second atom displaced by $\mathbf{d}_m$. The X-ray source is at S a distance R_0 from the origin, the incident ray making an angle φ_S with respect to $\mathbf{d}_m$. The detector is at point P a distance r from the origin (with exit angle φ_P) and r' from the second atom. The vector of length $r - d_m \cos\varphi_P$ corresponds to the plane-wave approximation for r'.

cells, the intensity reduces to

$$I_{3D}^{\text{plane}} = E_T E_T^* = \left(\frac{r_e}{r}\right)^2 E_I^2 F^2(\mathbf{q}) \left(\frac{\sin^2 \pi N_1 \mathbf{q}\cdot\mathbf{a}_1}{\sin^2 \pi \mathbf{q}\cdot\mathbf{a}_1}\right) \times \left(\frac{\sin^2 \pi N_2 \mathbf{q}\cdot\mathbf{a}_2}{\sin^2 \pi \mathbf{q}\cdot\mathbf{a}_2}\right)\left(\frac{\sin^2 \pi N_3 \mathbf{q}\cdot\mathbf{a}_3}{\sin^2 \pi \mathbf{q}\cdot\mathbf{a}_3}\right). \quad (8)$$

Equation (8) is the familiar result for the intensity scattered by a small crystal. If $\mathbf{q}$ matches a reciprocal-lattice vector $\mathbf{H}$, then Bragg's law is obtained. For the special case of specular reflection from a single atomic layer with $N_1 N_2$ unit cells (*i.e.* $N_3 = 1$), this further reduces to

$$I_{2D}^{\text{plane}} = (r_e/r)^2 E_I^2 F^2(\mathbf{q}) N_1^2 N_2^2. \quad (9)$$

(B) Spherical waves

We now repeat this analysis retaining the spherical waves, as first derived for specular reflection by Darwin (1914), and restated by James (1948) and Warren (1969). We consider first a single plane of the crystal with $N_1 N_2$ square unit cells. To be more general, the incident beam is emitted by a point source at S a distance R_o from the atom at $\mathbf{d}_o$. We shall later let $R_o \to \infty$ to recover the incident-plane-wave scenario. The full derivations are presented in Appendices *A* and *B*.

Again assuming perpendicular polarization, we examine first the reflected beam, where the source point S, the atom at $\mathbf{d}_o$ and the detector position P lie on a plane perpendicular to the surface (Fig. 2). The wave radiated by an atom at $\mathbf{d}_m = m_1\mathbf{a}_1 + m_2\mathbf{a}_2$ is

$$E_{m_1 m_2} = -(r_e/r_{m_1 m_2}) f E_I \times \exp\{i[2\pi k(R_{m_1 m_2} + r_{m_1 m_2}) - \omega t]\}, \quad (10)$$

where $R_{m_1 m_2}$ is the distance from s to the atom at $\mathbf{d}_{m_1 m_2}$ and $r_{m_1 m_2}$ is the additional distance to the detector position, P. The total field at P is obtained by summing the contributions from atoms at all $\mathbf{d}_m$ in the plane. This is done by comparing the total path length through $\mathbf{d}_m$ with that through the atom at $\mathbf{d}_o$ and expanding the difference in powers of a, the lattice constant. Retaining terms up to a^2, constructive interference is obtained and the summation reduces to Fresnel integrals when the reflection through $\mathbf{d}_o$ is specular. If R is allowed to go to infinity, the field at P is

$$E = -(1/\sin\varphi)(F r_e \lambda/a^2) E_I \times \exp\{i[2\pi k(r+R) - \omega t + \pi/2]\} = -i(Q/\sin\varphi) E_I \exp\{i[2\pi k(r+R) - \omega t]\}, \quad (11)$$

where $Q = r_e \lambda F(\mathbf{q})/a^2$ and φ is the angle of incidence. [Compare with equations (*A*10), (*A*11) and (*A*12) in Appendix *A*.] The corresponding intensity from this plane is

$$I_{2D}^{\text{spherical}} = (1/\sin^2\theta) Q^2 E_I^2. \quad (12)$$

Note that this reflected beam is a plane wave, as the intensity is independent of r.

The spherical-wave expression for non-specular diffraction from a periodicity a within a monolayer (Fig. 3) is derived in Appendix *B*:

$$E(P) = -i\{Q/[(1-\beta^2)(\beta^2 + \sin^2\varphi)]^{1/2}\} \times \mathcal{P} E_I \exp\{i[2\pi k(R+r) - \omega t]\}, \quad (B8)$$

where $\beta = n\lambda/2a$ and $\mathcal{P}$ is the polarization factor. In general, the intensity of a surface diffracted beam from a plane of atoms is

$$I_{2D} = \{Q^2/[(1-\beta^2)(\beta^2 + \sin^2\varphi)]\} \mathcal{P}^2 E_I^2. \quad (13)$$

In the above spherical-wave expressions, we have assumed that the atomic plane is much larger than the area of the first Fresnel zone, *i.e.* $N_1, N_2 \to \infty$. To complete the comparison with the plane-wave theory, we need an expression for the kinematic diffraction from a

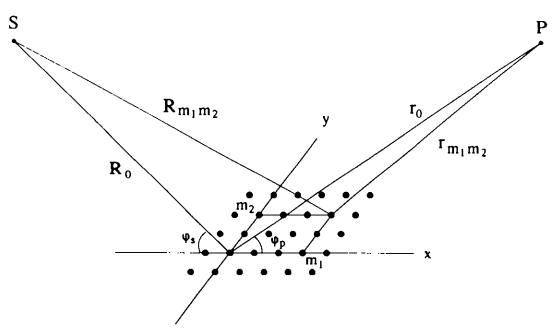

Fig. 2. Scattering geometry for reflectivity from a crystalline monolayer. The plane containing the source S, the detector P and the origin is perpendicular to the monolayer. The angles of incidence and reflection are φ_S and φ_P. The path length through the origin is $R_0 + r_0$, while through the lattice point at (m_1, m_2) it is $R_{m_1 m_2} + r_{m_1 m_2}$.

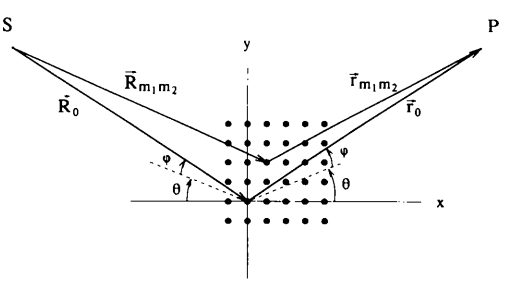

Fig. 3. Scattering geometry for surface Bragg diffraction. The incident and reflected beams make an angle φ to the crystal monolayer, *i.e.* the angle φ is to be viewed as coming out of the plane of the monolayer. The projection of these rays onto the surface (dashed lines) makes an angle θ with the x axis.

crystal containing N_3 atomic planes. This was derived by James (1948) and simply follows the procedure for adding plane waves already utilized in the plane wave model:

$$I_{3D} = \frac{Q^2\mathcal{P}^2E_I^2}{[(1-\beta^2)(\beta^2+\sin^2\varphi)]}\left(\frac{\sin^2\pi N_3\mathbf{q}\cdot\mathbf{a}_3}{\sin^2\pi\mathbf{q}\cdot\mathbf{a}_3}\right). \quad (14)$$

For the special case of specular reflectivity and/or diffraction, this simplifies somewhat to

$$I_{3D} = \frac{Q^2E_I^2}{\sin^2\varphi}\left(\frac{\sin^2\pi N_3\mathbf{q}\cdot\mathbf{a}_3}{\sin^2\pi\mathbf{q}\cdot\mathbf{a}_3}\right). \quad (15)$$

III. Discussion

We want first to directly compare the plane-wave and spherical-wave predictions for the intensity specularly reflected by a single monolayer:

$$\begin{aligned} I_{2D}^{\text{plane}} &= (r_e/r)^2E_I^2F^2(\mathbf{q})N_1^2N_2^2 \\ I_{2D}^{\text{spherical}} &= (1/\sin^2\theta)Q^2E_I^2 \\ &= (r_e/a)^2E_I^2F^2(\mathbf{q})[4/(qa)^2]. \end{aligned} \quad (16)$$

These two monolayer reflectivities are plotted as dashed lines in Fig. 4 for typical values of the parameters: $a = 3.0$ Å, $f = 30$, $\lambda = 1.5$ Å and $r = 1$m. The spherical-wave reflectivity assumes an infinite monolayer; the plane-wave reflectivity was calculated with N_1N_2 adjusted to match the spherical-wave reflectivity at normal incidence.

First, note that the intensity has the $1/\sin^2\theta$ behavior for the spherical waves. In the mathematical derivation, we can trace this extra factor to the angular dependence of the Fresnel-zone radii. Looking at it more physically, we can see that the difference in path lengths from the source point S to the detector point P through adjacent atoms is proportional to $\sin^2\varphi$. The major diameter of the central Fresnel zone, in which all of the atoms emit scattered waves that add constructively at P, is therefore proportional to $1/\sin^2\varphi$.

Second, we see that the plane-wave intensity diverges as the number of unit cells N_1N_2 increases, whereas the spherical-wave intensity rapidly approaches a fixed limit. This is due to the rapid oscillation in the phases of those waves that come from outside the first few Fresnel zones. This points out the critical parameter that separates these two models: the plane-wave theory is only appropriate when the effective crystal width is significantly less than L_1, the radius of the first Fresnel zone:

$$L_1 = (1/\sin\varphi)(\lambda r/2)^{1/2}. \quad (17)$$

Choosing typical values for the parameters ($r = 1$m, $\lambda = 1.5$ Å and $\varphi = 15°$) yields a radius of about 3×10^{-5} m (30 μm).

Third, we surprisingly find that the plane-wave model produces a spherical total scattered wave, while the spherical-wave model produces a plane wave. That is, when the incident beam is a plane wave (*i.e.* the distance R to the source S is much larger than the distance r to the detector P), the plane-wave result has an intensity that falls as r^{-2}, just like a spherical wave. On the other hand, the spherical-wave model leads to a specular-beam intensity that is independent of r, a genuine plane wave. In principle, this provides us with an experimental test to determine which model is appropriate for any diffracted signal. If the rays at the detector diverge with the crystal as the effective source, the plane-wave model is valid. If the effective source is at S, however the spherical-wave theory must be used.

Next, we examine the corresponding predictions for the specularly reflected intensity from a thin crystal with N_3 atomic planes:

$$\begin{aligned} I_{3D}^{\text{plane}} &= (r_e/r)^2E_I^2F^2(\mathbf{q})N_1^2N_2^2\left(\frac{\sin^2\pi N_3\mathbf{q}\cdot\mathbf{a}_3}{\sin^2\pi\mathbf{q}\cdot\mathbf{a}_3}\right) \\ I_{3D}^{\text{spherical}} &= (r_e/a)^2E_I^2F^2(\mathbf{q})[4/(qa)^2]\left(\frac{\sin^2\pi N_3\mathbf{q}\cdot\mathbf{a}_3}{\sin^2\pi\mathbf{q}\cdot\mathbf{a}_3}\right). \end{aligned} \quad (18)$$

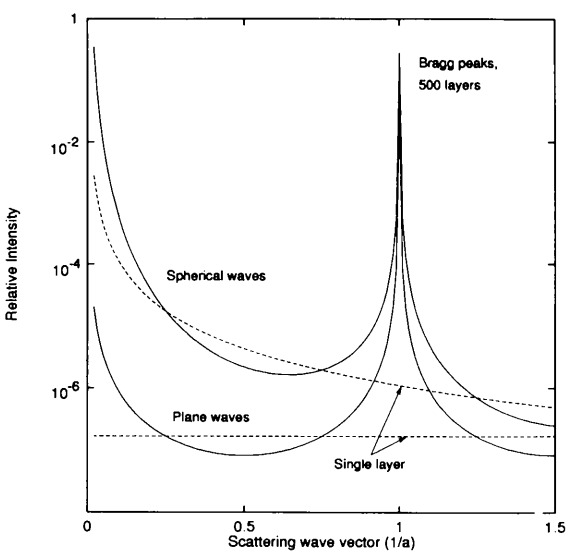

Fig. 4. Comparison of spherical- and plane-wave calculations. Dashed lines show the relative intensity I/I_0 for a single monolayer using (17) (see text). A simple square lattice was assumed with $a = 3.0$ Å, $f = 30$, $\lambda = 1.5$ Å and $r = 1$ m. The size of N_1N_2, the number of atoms in the plane for the plane-wave theory, was set to yield the same intensity at $\theta = 90°$ (normal incidence) as with the spherical-wave theory for an infinitely large monolayer. The solid lines are the reflectivities from $N_3 = 500$ such layers, using (19) and the same parameters as above. To simulate instrumental broadening, the rapidly oscillating factor ($\sin^2\pi N_3qa/\sin^2\pi qa$) was replaced by its average ($1/2\sin^2\pi qa$) except at the Bragg peak where the limiting value of N_3^2 was used. The two upper curves are for spherical waves and the two lower curves are the plane-wave results. Note the unmistakeable differences between the spherical- and plane-wave reflectivities at low q values.

These two reflectivities are plotted as the solid lines in Fig. 4, with the numbers of layers in the crystal, N_3, set to 500. The curves in Fig. 4 assume the entire crystal area is illuminated by the incident beam. The final factor in each formula arises from the summation of N_3 plane waves, since the wave reflected per monolayer in both theories is planar. The major distinction between these is again the factor of $1/(qa)^2$ from the spherical-wave monolayer reflectivity.

It is obvious that the diffracted intensities in the plane- and spherical-wave models are quite different. It was noted long ago (James, 1948), however, that for both models the total intensity received across the area of a sufficiently large detector is exactly the same at a Bragg reflection. For surface crystallography, it is important to show that this remains true in the tails of a Bragg reflection, *i.e.* at an arbitrary point on a reciprocal-lattice rod. This is derived in Appendix *C*: the errors in intensity and angular divergence cancel out, so that the plane-wave integrated intensity yields the correct spherical-wave result in all cases, not just at the Bragg peak.

In spite of this equivalence, it is important to emphasize that the plane-wave model is physically incorrect for sufficiently large domains. It is commonly assumed, for example, that in the Born approximation the differential cross section for the scattering of X-rays by a crystal is strictly proportional to the square of the Fourier transform of the scattering density:

$$(\mathrm{d}\sigma/\mathrm{d}\Omega) = r_e^2 V^2 |\rho_{\mathbf{H}}|^2 \qquad (19)$$

A derivation can be found in Landau, Lifschitz & Pitaevskii (1984), for example. Evidently, this perturbation theory breaks down if the lateral dimensions of the specimen (either monolayer or bulk) exceed the first Fresnel-zone diameter. Contrary to expectations, this failure of perturbation theory does not imply that a dynamical diffraction theory is necessary because diffracted beams orders of magnitude smaller than the incident beam exhibit the discrepancy (Fig. 4). [The dynamical theories of Darwin (1914) and Ewald (1917) explicitly assume spherical waves and the von Laue reformulation (1931) is completely equivalent.] Both plane- and spherical-wave models developed above are completely kinematic; a correct physical description of kinematic diffraction from large domains merely requires spherical waves, which we already know are dictated by Maxwell's equations. The simple form of (19) must, however, be modified by the additional $1/q^2$ of the diffracted intensity. That is, we lose the direct relationship between diffracted intensity and the Fourier transform of the scattering density but we retain the familiar plane-wave integrated intensity formulae.

IV. Concluding remarks

Specular reflection and in-plane diffraction formulae for X-ray scattering from a crystalline monolayer have been derived using the Darwin kinematic spherical-wave theory. A comparison of the plane-wave and spherical-wave models of kinematic diffraction has demonstrated significant differences in the calculated reflectivities. While the plane-wave theory predicts a reciprocal-space 'truncation rod' of uniform intensity, the correct spherical-wave theory for monolayers of sufficient size predicts a $1/q^2$ angular dependence. This illustrates the breakdown of the standard assumption that diffracted intensities are proportional to the square of the Fourier transform of the scattering density. While most previously published X-ray determinations of surface structure explicitly assume the validity of the plane-wave model (*e.g.* Robinson, 1986), even when the substrate is a nearly perfect crystal, the results are still generally valid because of the identical integrated intensities derived from the two models, both at Bragg peaks and far into the tails of the reflections.

The author thanks the Hamburger Synchrotronstrahlungslabor (HASYLAB) and the Universität Hamburg for the opportunity to teach a course on X-ray physics, where these ideas were first developed. Special thanks are due to Jin-Seok Chung for help with the figures and to Doon Gibbs for reading the manuscript. This work was supported by the National Science Foundation grant DMR 90-12785.

APPENDIX *A*
Reflected and transmitted beams

Although Darwin's original treatment of reflectivity from a plane assumed a uniform distribution of scatterers, we retain here the notion of discrete atoms distributed on a lattice. All of the following results are otherwise identical to those of Darwin (1914) [see also James (1948) and Warren (1969)]. We consider a square-planar array of identical atoms in the xy plane, with bond lengths a oriented along the x and y axes. As shown in Fig. 2, an X-ray source is located at S a distance R from the atom at the origin, making the angle φ_S with the monolayer along the $-x$ axis. The source distance R will later be made infinite to describe a plane wave. For simplicity, the incident wave at the origin $\mathbf{E}_I = \boldsymbol{\varepsilon}_I E_I \exp[i(2\pi kR - \omega t)]$ is polarized perpendicular to the scattering plane. The amplitude E_o of the wave scattered by the atom at the origin to the detector position P a distance r away and making the angle φ_P with the $+x$ axis is

$$E_o(P) = -(e^2/mc^2)(1/r) f E_I \exp\{i[2\pi k(R + r) - \omega t]\} \qquad (A1)$$

where e and m are the electron charge and mass, c is the speed of light in vacuum and f is the atomic scattering factor, which includes the form factor, dispersion and Debye–Waller-factor contributions. Now, consider an atom at the lattice position

$$\mathbf{d}_{m_1 m_2} = m_1 \mathbf{a}_1 + m_2 \mathbf{a}_2. \qquad (A2)$$

By assuming that $|\mathbf{d}|$ is much smaller than r and R, we can use the binomial expansion to write the path length from S to P through the lattice point $\mathbf{d}_{m_1 m_2}$ as

$$\begin{aligned}(R_{m_1m_2} + r_{m_1m_2}) &= R + r + m_1 a[\cos\varphi_S - \cos\varphi_P] \\ &\quad + (m_1 a)^2[(\sin^2\varphi_S)/2R + (\sin^2\varphi_P)/2r] \\ &\quad + (m_2 a)^2[1/2R + 1/2r] \\ &\equiv R + r + C_0 m_1 a \\ &\quad + C_1 m_1^2 a^2 + C_2 m_2^2 a^2 \qquad (A3)\end{aligned}$$

and the wave amplitude is

$$\begin{aligned}E_{m_1m_2} &= -(e^2/mc^2)(f/r_{m_1m_2})E_0 \exp(-i\omega t) \\ &\quad \times \exp\{-2\pi ik[R + r + C_0 m_1 a \\ &\quad + C_1 m_1^2 a^2 + C_2 m_2^2 a^2]\}. \qquad (A4)\end{aligned}$$

We now write the total field amplitude at P by summing over all lattice sites:

$$\begin{aligned}E &= -(e/mc^2)(f/r)E_0 \exp\{i[2\pi k(r + R) - \omega t]\} \\ &\quad \times \sum_{m_1=0}^{N_1-1} \exp\{2\pi ik[C_0 m_1 a + C_1 m_1^2 a^2]\} \\ &\quad \times \sum_{m_2=0}^{N_2-1} \exp(2\pi ikC_2 m_2^2 a^2), \qquad (A5)\end{aligned}$$

where we have replaced $r_{m_1m_2}$ by r in the prefactor of the exponential, which is valid if the distance to the detector position P is much larger than the sample dimensions. The last summation can be rewritten as a Fresnel integral and evaluated exactly in the limit that N_2 goes to infinity. The result will still be an excellent approximation to a finite crystal because of the rapid convergence of the sum

$$\begin{aligned}\sum_{m_2} \exp(2\pi ikC_2 m_2^2 a^2) &\to \int_{-\infty}^{+\infty} (1/a)\exp(2\pi ikC_2 x^2)\mathrm{d}x \\ &= (1/a)(4kC_2)^{-1/2}(1 + i), \qquad (A6)\end{aligned}$$

where we have used the identity

$$\int_0^{\infty} \exp[i(\pi/2)v^2]\mathrm{d}v = \tfrac{1}{2}(1 + i). \qquad (A7)$$

This is perhaps the most import result of the Darwin monolayer theory: the sum of spherical waves from an infinite number of atoms in a plane is finite. Now let us look at the other summation in (A5):

$$\begin{aligned}&\sum_{m_1} \exp\{2\pi ik[C_0 m_1 a + C_1 m_1^2 a^2]\} \\ &\quad = \sum_{m_1} \exp\left\{2\pi ik\left[(\cos\varphi_S - \cos\varphi_P)m_1 a \right.\right. \\ &\quad \left.\left. + \left(\frac{\sin^2\varphi_S}{2R} + \frac{\sin^2\varphi_P}{2r}\right)m_1^2 a^2\right]\right\}. \qquad (A8)\end{aligned}$$

We see at once that this reduces to the previous Fresnel sum if $\cos\varphi_P = \cos\varphi_S$, *i.e.* if the reflection is specular.* We can then write

$$\begin{aligned}\sum_{m_1} \exp(2\pi i\, kC_1 m_1^2 a^2) &\to \int_{-\infty}^{+\infty} (1/a)\exp(2\pi i\, kC_1 x^2)\mathrm{d}x \\ &= (1/a)(4kC_1)^{-1/2}(1 + i). \qquad (A9)\end{aligned}$$

With these results put into (A5), the field amplitude at the point P is

$$\begin{aligned}E &= -(e^2/mc^2)fE_0 \exp\{i[2\pi k(r + R) - \omega t] \\ &\quad \times (1/r)(1/a^2)[Rr/(R + r)](\lambda/2\sin\varphi)(1 + i)^2 \\ &= -(e^2/mc^2)(f/a^2\sin\varphi)[R\lambda/(R + r)]E_0 \\ &\quad \times \exp\{i[2\pi k(r + R) - \omega t + \pi/2]\}. \qquad (A10)\end{aligned}$$

For convenience, we replace the constant $R/(R + r)$ by unity, which is valid for a planar incident wave ($R \gg r$). Now define the factor Q:

$$\begin{aligned}Q &\equiv (e^2/mc^2)M\lambda f(2\varphi) \\ &= r_e \lambda M F(\mathbf{q}), \qquad (A11)\end{aligned}$$

where $M = 1/a^2$ is the atomic areal density and the form-factor contribution to the atomic scattering factor is explicitly denoted $f(2\varphi)$. In the second line, we have substituted the structure factor F for the atomic scattering factor f, which describes the scattering from an entire unit cell located at each Bravais-lattice point. Finally, we can write the field at P as

$$E(P) = -i(Q/\sin\varphi)E_0 \exp\{i[2\pi k(r + R) - \omega t]\}. \qquad (A12)$$

This expression has several noteworthy features. First, the amplitude does not diverge even for a monolayer of infinite size. Second, the amplitude also does not depend on r, the distance to the detector, when the incident beam is a plane wave. This shows that, for specular reflectivity, an infinite number of spherical waves coherently superpose to produce a plane wave of finite amplitude. Third, note that the factor i means that the phase of the total reflected beam is shifted by $\pi/2$ with respect to the individual wave scattered by the atom at the origin. Finally, the scattered-beam amplitude will be at least three orders of magnitude smaller than the incident-beam amplitude for typical values of the constants. This ensures that we are still very much in the kinematic regime, where the energy scattered into a reflected beam is a negligible fraction of the incident flux.

* In general, there are other valid solutions to $(\cos\varphi_S - \cos\varphi_P)m_1 a = n$. This is in fact the 'grating equation' for the orders of reflection from a linear diffraction grating. In other words, the corresponding reciprocal-lattice rods are due to diffraction from parallel rows of atoms behaving exactly as an optical grating.

APPENDIX B
Surface diffraction beams

We now take advantage of having discrete atoms distributed on a lattice in order to calculate diffraction from the atomic periodicities within the monolayer, *i.e.* surface diffraction. This subject was not treated by Darwin, no doubt due to the unlikelihood that such calculations could be compared with experiment. The scattering geometry, shown in Fig. 5, is oriented so that each row of atoms parallel to the x axis might produce a net field at P that can add constructively with the field from all the other rows.

As before, we want to write down the field at P due to the scattering from an atom at $\mathbf{d} = m_1 a\hat{\mathbf{i}} + m_2 a\hat{\mathbf{j}}$. One finds that

$$\begin{aligned} R^2_{m_1 m_2} &= R^2 + 2aR\cos\varphi[m_2\sin\theta + m_1\cos\theta] \\ &\quad + a^2[m_1^2 + m_2^2] \\ r^2_{m_1 m_2} &= r^2 + 2ar\cos\varphi[m_2\sin\theta - m_1\cos\theta] \\ &\quad + a^2[m_1^2 + m_2^2]. \end{aligned} \tag{B1}$$

With the use of the binomial expansion again and a combination of these two results, the total path length from S to P through the atom at $\mathbf{d}$ reduces to

$$\begin{aligned} R_{m_1 m_2} + r_{m_1 m_2} &= R + r + 2am_2\cos\varphi\sin\theta \\ &\quad + (a^2/2)[m_1^2 + m_2^2 - \cos^2\varphi(m_1^2\cos^2\theta \\ &\quad + m_2^2\sin^2\theta)][(r+R)/rR] \\ &\quad + \tfrac{1}{2}a^2\cos^2\varphi[(2/r)m_1 m_2\cos\theta\sin\theta \\ &\quad - (2/R)m_1 m_2\cos\theta\sin\theta]. \end{aligned} \tag{B2}$$

This has an especially simple form when we set $R = r$, *i.e.* for one-to-one focusing:

$$\begin{aligned} R_{m_1 m_2} + r_{m_1 m_2} &= R + r + 2m_2 a\cos\varphi\sin\theta \\ &\quad + (a^2/R)[m_1^2(1 - \cos^2\varphi\cos^2\theta) \\ &\quad + m_2^2(1 - \cos^2\varphi\sin^2\theta)]. \end{aligned} \tag{B3}$$

This is to be inserted into the expression for the total field re-radiated from all lattice points m_1, m_2 to the observation point P:

$$\begin{aligned} E(P) &= -\mathcal{P}E_I(e^2/mc^2)(f/r) \\ &\quad \times \sum_{m_1}\sum_{m_2}\exp\{-i[\omega t - 2\pi k(R_{m_1 m_2} + r_{m_1 m_2})]\} \\ &= -\mathcal{P}E_I(e^2/mc^2)(f/r)\exp\{i[2\pi k(R+r) - \omega t]\} \\ &\quad \times \sum_{m_2}\exp\{2\pi ik[2m_2 a\cos\varphi\sin\theta]\} \\ &\quad \times \exp\{2\pi ik[m_2^2(a^2/R)(1 - \cos^2\varphi\sin^2\theta)]\} \\ &\quad \times \sum_{m_1}\exp\{2\pi ik[m_1^2(a^2/R)(1 - \cos^2\varphi\cos^2\theta)]\}, \end{aligned} \tag{B4}$$

where $\mathcal{P} = \boldsymbol{\varepsilon}_I \cdot \boldsymbol{\varepsilon}$ is the polarization correction for dipole radiation. For the sum over m_2 to again have the form of a Fresnel sum, the first exponential factor must be a constant. This is ensured if

$$\begin{aligned} 2\pi k(2a\cos\varphi\sin\theta) &= (2\pi/\lambda)(2a\cos\varphi\sin\theta) \\ &= 2\pi n, \quad n = 0, \pm 1, \pm 2, \ldots \end{aligned}$$

or

$$2a\cos\varphi\sin\theta = n\lambda. \tag{B5}$$

This is Bragg's law for diffraction from a two-dimensional crystal. It arose as a direct result of requiring the summation in (B4) to have the form of a Fresnel sum. Deviations from this surface Bragg's law produce oscillations in the sum that rapidly reduce the total scattered amplitude. This expression is nothing more, of course, than requiring the in-plane component of the scattering wave vector to match the in-plane reciprocal-lattice vector: $\mathbf{q}_{\parallel} = a$. Since there is no constraint on the perpendicular component of $\mathbf{q}$, the Bragg condition is met for any $\mathbf{q}$ that terminates on a reciprocal-lattice rod perpendicular to the surface.

Next, we calculate the field at P at the Bragg condition:

$$\begin{aligned} E(P) &= -\mathcal{P}E_I(e^2/mc^2)(f/r)\exp\{i[2\pi k(R+r) - \omega t]\} \\ &\quad \times \sum_{m_2}\exp\{i(2\pi/\lambda)[m_2^2(a^2/R)(1 - \cos^2\varphi\sin^2\theta)]\} \\ &\quad \times \sum_{m_1}\exp\{i(2\pi/\lambda)[m_1^2(a^2/R)(1 - \cos^2\varphi\cos^2\theta)]\} \\ &= -\mathcal{P}E_I\exp\{i[2\pi k(R+r) - \omega t]\}(e^2/mc^2) \\ &\quad \times (f/r)(1/a^2)[(4/\lambda R)(1 - \beta^2)]^{-1/2} \\ &\quad \times [(4/\lambda R)(\sin^2\varphi + \beta^2)]^{-1/2} \\ &\quad \times \int_{-\infty}^{\infty}\exp[i(\pi/2)v^2]\mathrm{d}v \int_{-\infty}^{+\infty}\exp[i(\pi/2)u^2]\mathrm{d}u \\ &= -\mathcal{P}E_I\exp\{i[2\pi k(R+r) - \omega t]\}(e^2/mc^2) \\ &\quad \times (f/r)(1/a^2)(\lambda R/4) \\ &\quad \times [(1 - \beta^2)(\sin^2\varphi + \beta^2)]^{-1/2}(1+i)^2 \\ &= -\mathcal{P}E_I\exp\{i[2\pi k(R+r) - \omega t + \pi/2]\} \\ &\quad \times (e^2/mc^2)(f\lambda/2a^2) \\ &\quad \times [(1 - \beta^2)(\beta^2 + \sin^2\varphi)]^{-1/2}, \end{aligned} \tag{B6}$$

where $\beta = n\lambda/2a$. Note that instead of the $1/\sin\varphi$ dependence found in the specular beam, the monolayer diffraction amplitude is proportional to $1/[\beta^2 + (\sin\varphi)^2]^{1/2}$.

To compare directly with the von Laue plane-wave model and with the Darwin reflectivity in Appendix A, we must consider the scenario with an incident beam that is a plane wave. First, we let $R \to \infty$ in (B2), and again derive the surface Bragg's law by examining the linear

term in the exponential inside the Fresnel sum for the total field, $E(P)$. This term is

$$2aN_2 \cos\varphi \sin\theta[1 + (N_1 a/2r)\cos\varphi\cos\theta] \simeq 2aN_2 \cos\varphi \sin\theta. \quad (B7)$$

The correction term can be ignored as long as the sample dimensions are small compared with the detector distance. We therefore retain (B5) as the surface Bragg's law for incident plane waves also, and we find a total field amplitude at the detector which is twice as large as before:

$$E(P) = -i\{Q/[(1-\beta^2)(\beta^2 + \sin^2\varphi)]^{1/2}\} \times \mathcal{P}E_I \exp\{i[2\pi k(R+r) - \omega t]\}. \quad (B8)$$

APPENDIX C
Integrated intensity for monolayer diffraction

We consider a plane wave of intensity I_0 incident on a crystalline monolayer with orthogonal unit-cell vectors $\mathbf{a}_1$ and $\mathbf{a}_2$. The total energy scattered to the detector is

$$E(\theta) = \iint I(\theta)\mathrm{d}t\mathrm{d}A = \iint P(\theta)I_0\mathrm{d}t\mathrm{d}A, \quad (C1)$$

where θ is the angle of incidence, the time integration is over the measurement interval, $\mathrm{d}A$ is an area element, to be integrated over the face of the detector, and $P(\theta)$ is the normalized reflectivity of the monolayer. A quantity independent of the time interval and the incident intensity is the monolayer's 'reflecting power',

$$(1/I_0)[\partial E(\theta)/\partial t] = \int P(\theta)\mathrm{d}A. \quad (C2)$$

From (12), we have for spherical waves

$$P(\theta) = (Q^2/\sin^2\theta) = (1/\sin^2\theta)(r_e \lambda f/a_1 a_2)^2, \quad (C3)$$

where r_e is the classical electron radius, λ is the wavelength and f is the atomic scattering factor (including the form-factor correction). The corresponding result for the plane-wave approximation is

$$P(\theta) = \left(\frac{r_e}{r}\right)^2 f^2 \left(\frac{\sin^2\pi N_1 \mathbf{q}\cdot\mathbf{a}_1}{\sin^2\pi\mathbf{q}\cdot\mathbf{a}_1}\right)\left(\frac{\sin^2\pi N_2\mathbf{q}\cdot\mathbf{a}_2}{\sin^2\pi\mathbf{q}\cdot\mathbf{a}_2}\right), \quad (C4)$$

obtained from (8) by setting $N_3 = 1$.

The integrated intensity of a reflection is normally obtained by recording the X-ray intensity from a stationary detector with a large acceptance area, while the crystal is rotated through an angular range about the Bragg angle θ_B. This approach assumes that, at an increment $\Delta\theta$ above or below θ_B, the detected signal is negligible compared to the peak intensity. (The detector area also must be large enough to accept all of the radiation in the diffracted beam as it moves with changing θ.) This approach is not appropriate for monolayer diffraction, since $I(\theta)$ does not go through a maximum over any range $\Delta\theta$. If the monolayer is rotated, the detected signal will go through a peak only because the diffracted beam is moving across the acceptance area of the detector. In this case, the integrated intensity is

$$E = \iiint P(\theta)I_0\mathrm{d}t\mathrm{d}A\mathrm{d}\theta \simeq \Delta\theta \iint P(\theta_0)I_0\mathrm{d}t\mathrm{d}A, \quad (C5)$$

where $\Delta\theta$ is the angular acceptance of the detector. The approximation in the second line is valid for sufficiently small range $\Delta\theta$ about the midpoint θ_0.

For an integrated-intensity measured obtained by rotating the specimen through an angular range exceeding the detector acceptance $\Delta\theta$, the appropriately normalized reflecting power of the specimen is

$$(1/\Delta\theta I_0)[\partial E(\theta_0)/\partial t] = \int P(\theta_0)\mathrm{d}A. \quad (C6)$$

We denote by A_0 the area of the incident beam intercepted by the sample, making a 'footprint' of $A_0/\sin\theta$. In the spherical-wave model, the diffracted beam is a plane wave and hence a constant across the detector, so

$$\int P_{\mathrm{sph}}(\theta)\mathrm{d}A = Q^2 A_0/\sin^2\theta. \quad (C7)$$

For the plane-wave model, we substitute $\mathrm{d}A = r^2\mathrm{d}\beta\mathrm{d}\gamma$, where r is the distance to the detector and β and γ are orthogonal angular displacements (see Fig. 5):

$$\int P_{\mathrm{pl}}(\theta)\mathrm{d}A = r_e^2 f^2 \int\left(\frac{\sin^2\pi N_1\mathbf{q}\cdot\mathbf{a}_1}{\sin^2\pi\mathbf{q}\cdot\mathbf{a}_1}\right)\left(\frac{\sin^2\pi N_2\mathbf{q}\cdot\mathbf{a}_2}{\sin^2\pi\mathbf{q}\cdot\mathbf{a}_2}\right)\mathrm{d}\beta\mathrm{d}\gamma. \quad (C8)$$

Writing $\mathbf{q} = \mathbf{q}_{hk} + \Delta_{\mathbf{q}}$, where $\mathbf{q}_{hk}\cdot\mathbf{a}_1 = h$ and $\mathbf{q}_{hk}\cdot\mathbf{a}_2 = k$ correspond to being directly on the reciprocal-lattice rod, we also assume for simplicity that $\mathbf{a}_1$ lies in the diffraction plane and $\mathbf{a}_2$ is perpendicular to it.

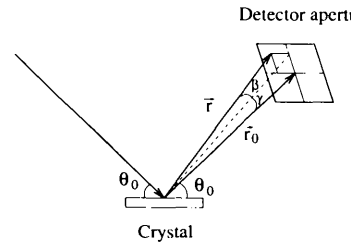

Fig. 5. Scattering geometry for specular ($\mathbf{r}_0$) and non-specular ($\mathbf{r}$) rays scattered by a specimen into a detector with a finite receiving aperture. The angle γ refers to displacements in the diffraction plane and β is in the orthogonal direction. The total number of X-rays recorded by such a detector is the integrated intensity, *i.e.* integrated across the face of the detector, and therefore over a range of β and γ values.

Then,

$$\Delta\mathbf{q}\cdot\mathbf{a}_1 = \Delta q_\gamma a_1 \sin\theta = [(a_1 \sin\theta/\lambda]\gamma$$
$$\Delta\mathbf{q}\cdot\mathbf{a}_2 = \Delta q_\beta a_2 = (a_2/\lambda)\beta$$

and

$$\int\left[\frac{\sin^2(\pi N_1 a_1 \sin\theta\gamma/\lambda)}{\sin^2(\pi a_1 \sin\theta\gamma/\lambda)}\right]\left[\frac{\sin^2(\pi N_2 a_2\beta/\lambda)}{\sin^2(\pi a_2\beta/\lambda)}\right]\mathrm{d}\beta\mathrm{d}\gamma$$
$$= (1/\sin\theta)N_1N_2\lambda^2/a_1a_2, \qquad (C9)$$

and

$$\int P_{\mathrm{pl}}(\theta)\mathrm{d}A = (1/\sin\theta)N_1N_2r_e^2f^2\lambda^2/(a_1a_2). \qquad (C10)$$

We now derive expressions for this reflecting power for two different experimental geometries. In the first case, the monolayer has infinite lateral extent and is illuminated by an incident beam of cross-sectional area A_0. For the spherical-wave model,

$$\int P_{\mathrm{sph}}(\theta)\mathrm{d}A = (Q^2A_0/\sin^2\theta) = (1/\sin^2\theta)(r_e\lambda fM)^2A_0, \qquad (C11)$$

where $M = 1/(a_1a_2)$ is the density of surface atoms. For plane waves, the area on the surface is $N_1a_1N_2a_2 = A_0/\sin\theta$, so

$$\int P_{\mathrm{pl}}(\theta)\mathrm{d}A = (1/\sin\theta)N_1N_2(r_ef\lambda)^2(1/a_1a_2)$$
$$= (1/\sin^2\theta)(r_e\lambda fM)^2A_0. \qquad (C12)$$

Note that the two models give identical reflecting powers, and hence the same integrated intensities. When the specimen is rotated by more than $\Delta\theta$, the integrated reflecting power is

$$\int_{\theta_1}^{\theta_2}\int P(\theta)\mathrm{d}A\mathrm{d}\theta = (\Delta\theta/\sin^2\theta)(r_e\lambda fM)^2A_0.$$

For the second case, we consider a specimen of finite area A_s that is completely irradiated by the incident plane-wave field. The effective area of the incident beam is therefore $A_o = A_s\sin\theta$. For spherical waves, we find

$$\int P_{\mathrm{sph}}(\theta)\mathrm{d}A = (Q^2A_0/\sin^2\theta)$$
$$= (1/\sin\theta)(r_e\lambda fM)^2A_s, \qquad (C13)$$

and for plane waves

$$\int P_{\mathrm{pl}}(\theta)\mathrm{d}A = (1/\sin\theta)N_1N_2(r_ef\lambda)^2(1/a_1a_2)$$
$$= (1/\sin\theta)(r_e\lambda fM)^2A_s. \qquad (C14)$$

Finally, we consider a crystal made up of N_3 monolayers with lattice constant $\mathbf{a}_3$. For spherical waves, we have from (16)

$$P_{\mathrm{sph}}(\theta) = (Q^2a_0/\sin^2\theta)\left(\frac{\sin^2\pi N_3\mathbf{q}\cdot\mathbf{a}_3}{\sin^2\pi\mathbf{q}\cdot\mathbf{a}_3}\right). \qquad (C15)$$

If the crystal is rocked through the Bragg angle, then

$$\left(\frac{1}{I_0}\right)\left(\frac{\partial E}{\partial t}\right) = \int_{\theta_1}^{\theta_2} P_{\mathrm{sph}}(\theta)\mathrm{d}\theta$$
$$\simeq \left(\frac{Q^2A_0}{\sin^2\theta_B}\right)\left(\frac{\lambda}{2\cos\theta_B}\right)$$
$$\times \int_{-\infty}^{+\infty}\frac{\sin^2\pi N_3q_3a_3}{\sin^2\pi q_3a_3}\mathrm{d}q_3$$
$$= \frac{N_3\lambda Q^2A_0}{2a_3\sin^2\theta_B\cos\theta_B}$$
$$= \frac{r_e^2f^2\lambda^3\delta V}{v_a^2\sin 2\theta_B}$$
$$\equiv R_B, \qquad (C16)$$

where we have used $\mathrm{d}q = (2\cos\theta/\lambda)\mathrm{d}\theta$, $v_a = a_1a_2a_3$ (the unit-cell volume) and $\delta V = (A_0/\sin\theta)N_3a_3$ (the irradiated volume of the crystal). If the range $\Delta\theta$ does not include a Bragg angle, then we simply replace $\sin^2\pi N_3q_3a_3$ by 1/2, its average:

$$\left(\frac{1}{I_0}\right)\left(\frac{\partial E}{\partial t}\right) = \frac{Q^2A_0}{\sin^2\theta}\,\frac{\Delta\theta/2}{\sin^2(\pi q_3a_3)}$$
$$= \frac{Q^2A_0\lambda}{2\sin^2\theta\cos\theta}\,\frac{\Delta q}{2\sin^2(\pi q_3a_3)}$$
$$= \frac{1}{N_3}\,\frac{\Delta qa_3}{2\sin^2(\pi q_3a_3)}\left(\frac{\sin 2\theta_B}{\sin 2\theta}\right)R_B. \qquad (C17)$$

This is the reflecting power of a segment Δq_3 about the point q_3 along a reciprocal-lattice rod, where $\Delta q_3 = (2\cos\theta/\lambda)\Delta\theta$ is determined by the angular acceptance $\Delta\theta$ of the detector. Because the reflecting power of a monolayer is the same for both the plane- and spherical-wave models [(C11) and (C12)], it will remain the same for a crystal of N_3 layers since in both models the effect of multiple monolayers is simply the factor

$$\left(\frac{\sin^2\pi N_3\mathbf{q}\cdot\mathbf{a}_3}{\sin^2\pi\mathbf{q}\cdot\mathbf{a}_3}\right),$$

as shown in (18). In summary, we find:

Monolayer:

$$\int P(\theta)\mathrm{d}A\mathrm{d}\theta = (\Delta\theta/\sin^2\theta)(r_e\lambda fM)^2A_0.$$

Crystal, Bragg:

$$\int P(\theta)\mathrm{d}A\mathrm{d}\theta = (r_e^2f^2\lambda^3\delta V)/v_a^2\sin 2\theta_B \equiv R_B.$$

Crystal, off-Bragg:

$$\int P(\theta)\mathrm{d}A\mathrm{d}\theta = (1/N_3)[\Delta q_3 a_3/2\sin^2(\pi q_3 a_3)](\sin 2\theta_B/\sin 2\theta)R_B.$$

References

ANDREWS, S. R. & COWLEY, R. A. (1985). *J. Phys. C*, **18**, 6427–6439.
DARWIN, C. G. (1914) *Philos. Mag.* **27**, 315–333, 675–690.
EWALD, P. P. (1917). *Ann. Phys. (Leipzig)*, **54**, 519–597.
EWALD, P. P. (1940). *Proc. Phys. Soc. London*, **52**, 167–174.
FRIEDRICH, W., KNIPPING, P. & VON LAUE, M. (1913). *Ann. Phys. (Leipzig)*, **41**, 971–988.
JAMES, R. W. (1948). *The Optical Principles of the Diffraction of X-rays. The Crystalline State*, Vol. II, edited by SIR LAWRENCE BRAGG. London: Bell.
LANDAU, L. D., LIFSCHITZ, E. M. & PITAEVSKII, L. P. (1984). *Electrodynamics of Continuous Media*, 2nd ed., ch. 16. Oxford: Pergamon.
LAUE, M. VON (1913). *Ann. Phys. (Leipzig)*, **41**, 989–1002.
LAUE, M. VON (1931). *Ergeb. Exackten Naturwiss.* **10**, 133.
LAUE, M. VON & TANK, F. (1913). *Ann. Phys. (Leipzig)*, **41**, 1003–1011.
ROBINSON, I. K. (1986). *Phys. Rev. B*, **33**, 3830–3836.
WARREN, B. E. (1969). *X-ray Diffraction*. New York: Addison-Wesley. Reprinted by Dover Publications (1990).

Acta Cryst. (1995). A**51**, 268–270

A Tangent Formula Derived from Patterson-Function Arguments. II. Practical Tests with Single-Crystal Intensity Data

BY J. RIUS, J. SAÑÉ AND C. MIRAVITLLES

Institut de Ciència de Materials de Barcelona (CSIC), Campus de la UAB, 08193 *Cerdanyola, Catalunya, Spain*

AND J. M. AMIGÓ AND M. M. REVENTÓS

Department de Geologia, Universitat de València, 46100 *Burjassot, Spain*

(*Received* 24 *June* 1994; *accepted* 20 *September* 1994)

Abstract

A series of test calculations of the tangent formula derived from Patterson-function arguments [Rius (1993). *Acta Cryst.* A**49**, 406–409] using single-crystal intensity data is presented. This new tangent formula has been compared with the results reported [Sheldrick (1990). *Acta Cryst.* A**46**, 467–473] for (*a*) the tangent formula incorporating the most reliable negative quartets and (*b*) its extension to the phase-annealing method. The success rate of the new tangent formula is an order of magnitude higher than that of (*a*), is better than that of (*b*) when the origin can float in at least one direction, and is similar to that of (*b*) for other space groups.

1. Introduction

Nowadays, the applicability of *direct methods* to larger crystal structures constitutes an active research field. Since the number of correct solutions produced by direct methods tends to decrease with increasing size of the structure, it is interesting to know which tangent formulas are most effective. Eventually, these tangent formulas or the functions that they maximize or minimize could be selected for further development. Logically, to determine their relative efficiencies, the different tangent formulas have to be tested on the same structures. Unfortunately, this has not been common practice; to date, each new tangent formula has been tested using an arbitrary selection of structures. In order to modify this situation, the test structures given by Sheldrick (1990) have been selected as 'reference' structures in this work. In this way, besides testing the tangent formula derived from Patterson-function arguments, it has also been possible to compare it with the tangent formula that incorporates the most reliable negative quartets. A brief introduction to both tangent formulas follows.

1.1. *The tangent formula incorporating the most reliable negative quartets*

Most multisolution direct-methods procedures (Germain & Woolfson, 1968) are based on the maximization of a certain function expressed in terms of the collectivity Φ of phases of the reflections with large E's (the basis set). The simplest function of Φ

$$Z(\Phi) = \sum_{\mathbf{h}}\sum_{\mathbf{h}'} E_{-\mathbf{h}}E_{\mathbf{h}'}E_{\mathbf{h}-\mathbf{h}'}\cos\Phi_3(\mathbf{h},\mathbf{h}') \qquad (1)$$

follows from the product of all the conditional probability distributions of triplets that only involve

©1995 International Union of Crystallography
Printed in Great Britain – all rights reserved